Journal of Anatomy

J. Anat. (2013) **223**, pp610–628 doi: 10.1111/joa.12121

Three-dimensional moment arms and architecture of chimpanzee (*Pan troglodytes*) leg musculature

Nicholas B. Holowka[1] and Matthew C. O'Neill[2]

[1]*Interdepartmental Doctoral Program in Anthropological Sciences, Stony Brook University, Stony Brook, NY, USA*
[2]*Department of Anatomical Sciences, Stony Brook University School of Medicine, Stony Brook, NY, USA*

Abstract

The muscular and skeletal morphology of the chimpanzee ankle and foot differs from that of humans in many important respects. However, little information is available on the moment arms and architecture of the muscles that function around chimpanzee ankle and foot joints. The main goals of this study were to determine the influence of changes in leg and foot position on the moment arms of these muscle–tendon units (MTUs), and provide new measurements of their architecture. Three-dimensional moment arm data were collected from two adult, cadaveric *Pan troglodytes* specimens for 11 MTUs that cross the ankle and foot joints. Tendon-excursion measurements were made throughout the full range of plantarflexion–dorsiflexion (PF–DF) and eversion–inversion (EV–IN), including repeated measurements for mm. gastrocnemius at 0°, 45°, 90° and 135 ° of knee flexion. The total range of motion was calculated from three-dimensional joint motion data while ensuring that foot movement was restricted to a single plane. Measurements of muscle mass, fascicle length, pennation angle and physiological cross-sectional area were then collected for each MTU. Our results demonstrate that joint position has a significant effect on moment arm lengths, and that in some cases this effect is counterintuitive. These new data contribute to filling a significant gap in previously published chimpanzee moment arm data, providing a comprehensive characterization of the MTUs that move the chimpanzee ankle and foot joints. They also provide empirical support to the notion that chimpanzees have larger ranges of motion at these joints than humans. Comparison of osteometric estimates of moment arm lengths to direct tendon-excursion measures provides some guidance for the use of skeletal features in estimations of PF–DF moment arms. Finally, muscle architecture data are consistent with the findings of previous studies, and increase the sample size of the chimpanzee data that are currently available.

Key words: ankle; chimpanzee; foot; moment arm; muscle; range of motion; tendon-excursion method.

Introduction

The structure of the human ankle and foot differs from that of apes and early hominins in many important respects (Lewis, 1980c; Stern & Susman, 1983; Latimer et al. 1987; Lovejoy et al. 2009; Zipfel et al. 2011), including the presence of longer plantarflexor (PF) moment arms and reduced joint mobility (Susman et al. 1984; Thorpe et al. 1999). These traits are among a suite of adaptations that allow the human foot to function as a rigid lever during bipedal walking (Bojsen-Møller, 1979; Susman, 1983), and as a compliant spring during running (Ker et al. 1987). Chimpanzees and other African apes, in contrast, appear to possess more mobile ankles and feet (Elftman & Manter, 1935a,b; Lewis, 1980a,b), which must therefore be capable of force generation over a wider range of leg and foot positions. However, to date, the effects of chimpanzee knee and ankle joint position on the three-dimensional moment-generating capabilities of the muscle–tendon units (MTUs) acting about the ankle and foot have not been fully investigated. Such data are essential for understanding the effect of skeletal morphology on MTU function, as well as for generating accurate estimates of muscle–tendon force and work output in dynamic analyses (Yamazaki et al. 1979; Thorpe et al. 2004; Sockol et al. 2007; Pontzer et al. 2009).

Moment arm length determines the amount of muscle force required to counter a given joint moment. The geometric definition of a moment arm is the perpendicular distance between the line of action of a MTU and the axis of rotation of the joint upon which the MTU acts. For a given MTU, this distance changes as a joint moves through its full range of motion. As a consequence, moment arm lengths

Correspondence
Nicholas B. Holowka, Interdepartmental Doctoral Program in Anthropological Sciences, Stony Brook University, Stony Brook, NY 11794-4364, USA. T: +(607) 279 5428; E: nicholas.holowka@stonybrook.edu

Accepted for publication *5 September 2013*
Article published online *2 October 2013*

often do not remain constant across joint positions. Two different methods have been devised to measure changes in moment arm length over a range of joint positions: the geometric-measurement method and the tendon-excursion method. For the geometric-measurement method, radiographic, computed tomography (CT), magnetic resonance or ultrasound images of a joint are collected at set intervals over a range of positions. The distance between the MTU line of action and an assumed joint center of rotation is then measured from each image (An et al. 1984; Rugg et al. 1990; Polk, 2002). The use of osteometrics to estimate moment arm lengths represents a simplified version of this method, and has been employed in many studies of locomotor or manipulative capabilities in living and fossil taxa (e.g. Schultz, 1963; Fleagle, 1976; Trinkaus, 1983; Strasser, 1992; Drapeau, 2004; Young, 2005; Raichlen et al. 2011). However, the accuracy of the geometric-measurement method is somewhat limited, because the MTU line of action and the joint center of rotation must be approximated (An et al. 1984; Spoor & van Leeuwen, 1992). In contrast, the tendon-excursion method involves the measurement of MTU excursion during angular motion at a joint. The derivative of the relationship between these variables provides instantaneous moment arm values across joint angles. This method follows the geometric law that when the radius of a circle rotates through one radian, the length of the arc traveled by any point on the radius will be equal to the distance between that point and the center of the circle. In the case of joint motion, to move a limb segment one radian, a tendon must be moved a distance equivalent to the perpendicular distance between the path of the tendon and the joint center of rotation. So, the derivative of the relationship between tendon excursion and joint angular excursion provides a measure of the true moment arm distance (Brand et al. 1975; An et al. 1983). Hence, no *a priori* knowledge of the MTU insertion or the joint center of rotation is needed.

Recent studies of ape moment arms have used the tendon-excursion method to document marked interspecific variation for many limb muscles, including those of the leg (Payne et al. 2006b; Channon et al. 2010). In the only such study of the common chimpanzee, Thorpe et al. (1999) measured the moment arms of the triceps surae muscles (i.e. m. gastrocnemius lateralis, m. gastrocnemius medialis and m. soleus) over the full range of PF–dorsiflexion (DF). However, these three MTUs have unique origins and, unlike in humans, chimpanzee gastrocnemius and soleus muscles maintain distinct bellies for most of the length of the leg (Swindler & Wood, 1973; Prejzner-Morawska & Urbanowicz, 1981). This raises the possibility that mm. gastrocnemius and m. soleus exhibit differences in their moment arm functions, especially for motion in non-sagittal planes. Further, Thorpe et al. (1999) did not consider the effect of knee position on the two-joint mm. gastrocnemius, nor did they collect data from any of the deep plantarflexors, peroneals or dorsiflexors. The main aim of this study, then, is to address this gap by evaluating the effect of joint position during motion in multiple planes on the force and moment-producing capabilities of all of the MTUs that cross the ankle in chimpanzees. Along with previous studies (Payne et al. 2006b; Channon et al. 2010), the data provided here will contribute to characterizing leg MTU moment arms across ape species. Additionally, this study involves direct measurements of chimpanzee ankle joint total ranges of motion, which is a topic of considerable interest (Stern & Susman, 1983; Latimer et al. 1987; DeSilva, 2009; Venkataraman et al. 2013), but for which little quantitative data are actually available from intact hind limbs.

The maximum moment-producing capabilities at the ankle are also dependent on the cross-sectional area of muscle that is available for force output. Muscle cross-sectional area is defined by its mass and architecture, including its average fascicle length and fascicle pennation angle (Alexander & Vernon, 1975; Lieber, 2010). As such, a second aim of this study is to provide new data on the architecture of the chimpanzee leg musculature. Muscle architecture data from the hind limbs of common chimpanzees (Thorpe et al. 1999; Nagano, 2001; Carlson, 2006; Myatt et al. 2011; Oishi et al. 2012) and other apes (Payne et al. 2006a; Channon et al. 2009) are still quite rare, and continued dissemination of new data is essential to elucidating intraspecific and interspecific variation as well as size-scaling patterns.

Materials and methods

Specimens and dissection

We collected data from an adult male ('Chimp A') and an adult female ('Chimp B') common chimpanzee (*Pan troglodytes troglodytes*), previously used in lab-based research (Table 1). The right hind limb of each individual had been disarticulated at the hip joint and fresh-frozen at about −20 °C at death until dissection. Both hind limb specimens were free of visible pathology. It should be noted that the body masses at death of Chimps A and B both exceed the mean, sex-specific body masses reported for wild-shot chimpanzees (Smith & Jungers, 1997). However, both individuals are within the mass range of a recent locomotion study involving captive adult chimpanzees (Sockol et al. 2007). In addition, both Chimps A and B possess femoral head diameters above the sex-specific averages reported for individuals of their species (M = 3.49 cm, F = 3.17 mm; Jungers & Susman, 1984). Femoral head size is a skeletal correlate of body size, so the large diameters measured in Chimps A and B suggest that the high masses of these individuals are actually reflective of relatively large body sizes, and not necessarily poor health or inactivity.

For each specimen, we removed the skin and fascia of the thigh and leg to a level just proximal to the talocrural joint then dissected the MTUs of the thigh free from their attachments. For the remaining 11 MTUs that cross the ankle joint (Table 2), we undertook the following steps. (i) We dissected the MTU from its origin, and sowed a silk suture (Prolene Monofilament; Ethicon, Somerville, NJ, USA) to its distal tendon; one suture was used to represent the mechanical action of each MTU. (ii) We marked a point

Table 1 Specimen information.

	Chimp A	Chimp B
Subject specs		
Sex	Male	Female
Age (years)	13	17
Mass (kg)	63.4	81.3
Cause of death	Pneumonia, heart attack	Pulmonary embolism
Morphometrics		
Femoral head diameter (cm)*	3.53	3.28
Femur length (cm)†	27.5	29.9
Tibia length (cm)‡	24.9	25.5
Foot length (cm)§	24.4	22.4
Foot width (cm)¶	6.1	5.3

*Measured as the maximum superior–inferior diameter of the femoral head.
†Measured from the top of the femoral head to the inferior surface of the lateral femoral condyle.
‡Measured from the medial condyle to the distal tip of the medial malleolus.
§Measured as the distance from the posterior calcaneus to the tip of the third digit.
¶Measured as the distance between the heads of the second and fifth metatarsals.

Table 2 Muscle groups and abbreviations.

Muscle	Abbreviation
Superficial plantarflexors	
Gastrocnemius lateralis	GL
Gastrocnemius medialis	GM
Soleus	SL
Deep plantarflexors	
Flexor digitorum fibularis	FDF
Flexor digitorum tibialis	FDT
Tibialis posterior	TP
Peroneal muscles	
Peroneus brevis	PB
Peroneus longus	PL
Dorsiflexors	
Extensor digitorum longus	EDL
Extensor hallucis longus	EHL
Tibialis anterior	TA

representing the muscle–tendon origin on the skeleton; for MTUs with broad origins, we identified and marked the approximate attachment area centroid. (iii) We constructed suture anchors from screws and vinyl tubing, and affixed them to the bone at each origin point. We threaded the sutures through the tubing such that the anchors maintained the proper line of action of each suture across the ankle and throughout the full range of joint motion.

Kinematics

Once dissected, we mounted the femur, tibia-fibula and foot in a custom-built jig that enabled simultaneous measurements of MTU length change and hind limb joint position (Fig. 1a). The femur and tibia-fibula were held stationary by clamps to avoid unwanted motion during ankle movements. Once the hind limb was firmly mounted, we fed each suture through a pulley fastened to the jig frame and secured it to an 8-oz lead weight. The weights were heavy enough to maintain tension on the sutures (and their associated tendons) throughout joint movements, as well as overcome any friction encountered at the anchors or pulleys. A spherical marker (1.5 cm diameter) was attached to the bottom of each weight in order to track its vertical displacement due to changes in joint position (Fig. 1b). To track changes in three-dimensional joint position, we also affixed spherical markers to the leg and foot segments. For the leg, we glued these markers to the tops of bone screws inserted into the medial side of the medial tibial condyle, the lateral side of the fibular head and the lateral side of the fibular malleolus; for the foot, we affixed the markers and bone screws at the lateral side of the calcaneal tuberosity, and to the medial and lateral sides of the heads of the second and fifth metatarsals, respectively. To enable passive foot manipulation, we attached a rigid board to the forefoot using tightly wrapped cloth tape to restrict motion distal to the metatarsal bases, then manually moved the foot in a manner that allowed motion to occur at the transverse tarsal, subtalar and talocrural joints.

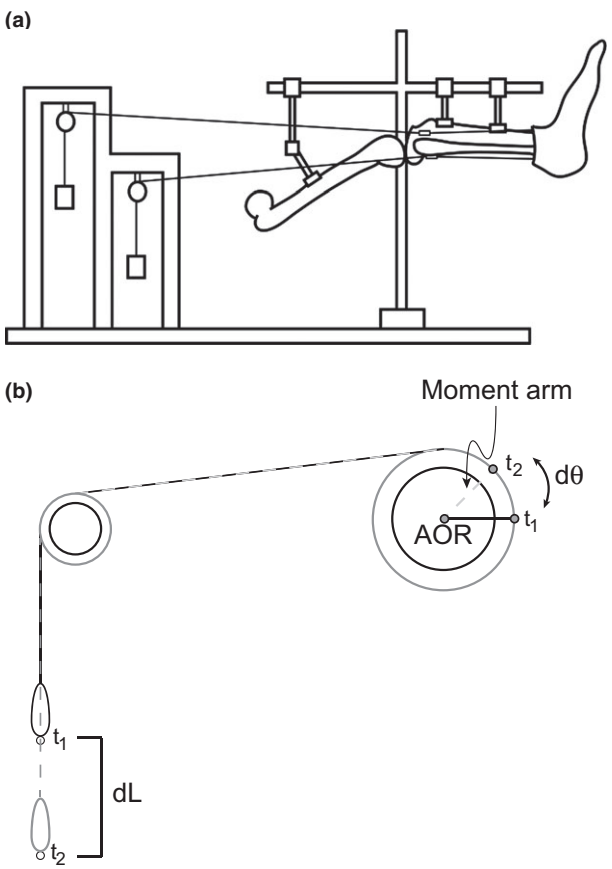

Fig. 1 Schematics of (a) the apparatus used to measure MTU moment arms, and (b) the derivation of MTU moment arm length. Moment arm length [distance from the MTU insertion (t) to the joint axis of rotation (AOR)] is calculated as the change in joint angle (dθ) with respect to MTU excursion distance (dL).

Following previous three-dimensional kinematic studies (Leardini et al. 2007), we defined ankle and foot motion as occurring about three orthogonal axes: a mediolateral axis (PF–DF); an anteroposterior axis [eversion–inversion (EV–IN)]; and a superoinferior axis [abduction–adduction (AB–AD)]. It is well known that PF–DF consists almost entirely of motion at the talocrural joint; however, EV–IN and AB–AD of the foot are composite motions that occur mainly at the subtalar and transverse tarsal joints (Elftman & Manter, 1935b; Lewis, 1980b). In this study, EV–IN and AB–AD reflect the net motion (rotation and displacement) of multiple skeletal elements proximal to the tarsometatarsal joints. Because each of the three above-mentioned ankle and foot motions occur about different axes of rotation, MTUs are expected to have different moment arm lengths depending on the axis about which joint motion is taking place.

We anticipated that the ankle moment arms of the gastrocnemius would change length as a function of knee flexion, because these MTUs cross both the knee and ankle joints. To evaluate this expectation, we measured m. gastrocnemius lateralis and medialis tendon excursion during PF–DF while the knee was fixed in 0° (full extension), 45°, 90° and 135° of flexion. We then measured tendon excursion for all MTUs while the foot was moved through its full range of PF–DF, EV–IN and AB–AD. Each foot manipulation trial consisted of one cycle through the full range of motion in one plane, while the foot was maintained at neutral position in the two orthogonal planes. For example, in EV–IN, ankle motion was constrained to rotation about the anteroposterior axis of the foot, while minimizing whatever simultaneous PF–DF or AB–AD might naturally occur. We used three trials from each motion to calculate the tendon displacement vs. joint angular motion curves for all muscles in both specimens.

In attempting to determine moment arms during superoinferior axis motion (AB–AD), we observed significant kinematic crosstalk (Piazza & Cavanagh, 2000) with PF–DF and EV–IN. That is, analysis of joint kinematics from these trials indicated that motion about this axis was accomplished via significant out of plane motion. As shown in Fig. 2, a large proportion of the total motion that occurred during AB–AD trials was outside of the desired plane, as compared with only a minimal amount of out of plane motion during the PF–DF and EV–IN trials. AB–AD occurs mainly at the subtalar and transverse tarsal joints, which possess axes of rotation that are likely to be slightly oblique to the long axis of the foot, so limiting motion solely to a superoinferior axis in these joints was not possible. Over concern that MTU excursion during AB–AD trials might actually result from motion in multiple planes, we excluded these trials from analysis.

We used a four-camera motion capture system to simultaneously record the movement of all hind limb and weight markers at 100 Hz during each passive manipulation. We calibrated cameras using a 36-point calibration frame with direct linear transformation in ProAnalyst (Xcitex Motion Procapture, Boston, MA, USA). We took an initial calibration shot to establish the neutral position of the ankle and foot in three dimensions. We filtered the marker coordinate data with a low-pass fourth order Butterworth filter using a 6-Hz cut-off frequency. We determined the cut-off frequency by performing residual analyses of the raw data from several selected trials (Winter, 2005). We then used the filtered data to calculate angular motion based on an XYZ Cardan rotation sequence (Hamill & Selbie, 2004; Sinclair et al. 2012).

Moment arm derivation and statistical model selection

We calculated MTU length change from the vertical displacement of the weight-attached markers. We then used polynomial regressions to determine a best-fit curve for the displacement vs. joint angles of each MTU. We fit first-, second- and third-order curves to the combined data from all three trials for a given motion, following the approach taken by several recent studies (Klein et al. 1996; Graham & Scott, 2003; Payne et al. 2006b). Previous moment arm studies have resorted to different methodologies for determining the proper order of the polynomial used for these regressions (Hintermann et al. 1994; Hughes et al. 1998; Delp et al. 1999), and no standardized method currently exists. Herein, we used statistical model selection – the Akaike information criterion (AIC) – to identify the best-fitting polynomial order. AIC values provide a measure of the relative strength of different model fits, such that the preferred model is the one with the lowest AIC value (Akaike, 1974; Sokal & Rohlf, 2012). We calculated the moment arm equation as the first derivative of the selected polynomial curve. In addition, we only derived moment arm equations from curves with $R^2 > 0.70$. We used this threshold value to avoid calculating moment arms in cases where the true relationship between MTU excursion and angular motion was not clearly defined in the data. This value was selected because previously published human and ape moment arm studies report MTU excursion vs. angular motion equations with R^2 values above this threshold (Klein et al. 1996; Thorpe et al. 1999; Payne et al. 2006b).

Osteometric measurements

In studies of primate ankle evolution, 'calcaneal tuber length' (Trinkaus, 1983; Raichlen et al. 2011) and the 'pedal power arm' (Schultz, 1963; Strasser, 1992) have both been used as osteometric estimates of moment arm length of the superficial plantarflexors. To directly evaluate the accuracy of these two metrics for predicting true moment arm lengths, we CT-scanned the foot and ankle of Chimps A and B using a GE Lightspeed CVT scanner prior to dissection. Serial scans of each individual were collected at a slice thickness of 0.625 mm (voltage: 140 kV; current: 120 mA), then imported into Avizo (VSG; Visualization Sciences Group, Burlington, MA, USA) for three-dimensional reconstruction. We rendered models of the intact skeletal elements and used them to measure 'calcaneal tuber length' [maximum distance from the posterior surface of the calcaneal tuberosity to the distal edge of the posterior talar facet on the calcaneus (Raichlen et al. 2011)] and 'pedal power arm' ['calcaneal tuber length' minus half the distance between the proximal and distal edges of the posterior talar facet (Strasser, 1992)]. We also devised an osteometric dimension on the talus to approximate the PF–DF moment arm of the deep plantarflexors: half the distance between the anterior and posterior surfaces of the talar trochlea. We conceived this dimension based on the location of the groove for m. flexor digitorum fibularis, which is directly posterior to the trochlear surface of the talus, where most PF–DF motion is expected to occur. This measurement assumes that the tendons of the deep plantarflexors will cross the talocrural joint exactly at this groove, and that the joint center of rotation during PF–DF is located midway across the anteroposterior length of the talar trochlea.

Muscle architecture

Prior to measurement of muscle architecture variables, we cleaned each muscle of loose fascia and fat, and blotted it dry. We then weighed the muscle to the nearest 1.0 g using a digital scale. To determine average fascicle length, we bisected each muscle from its distal tendon to its proximal attachment along the length of its

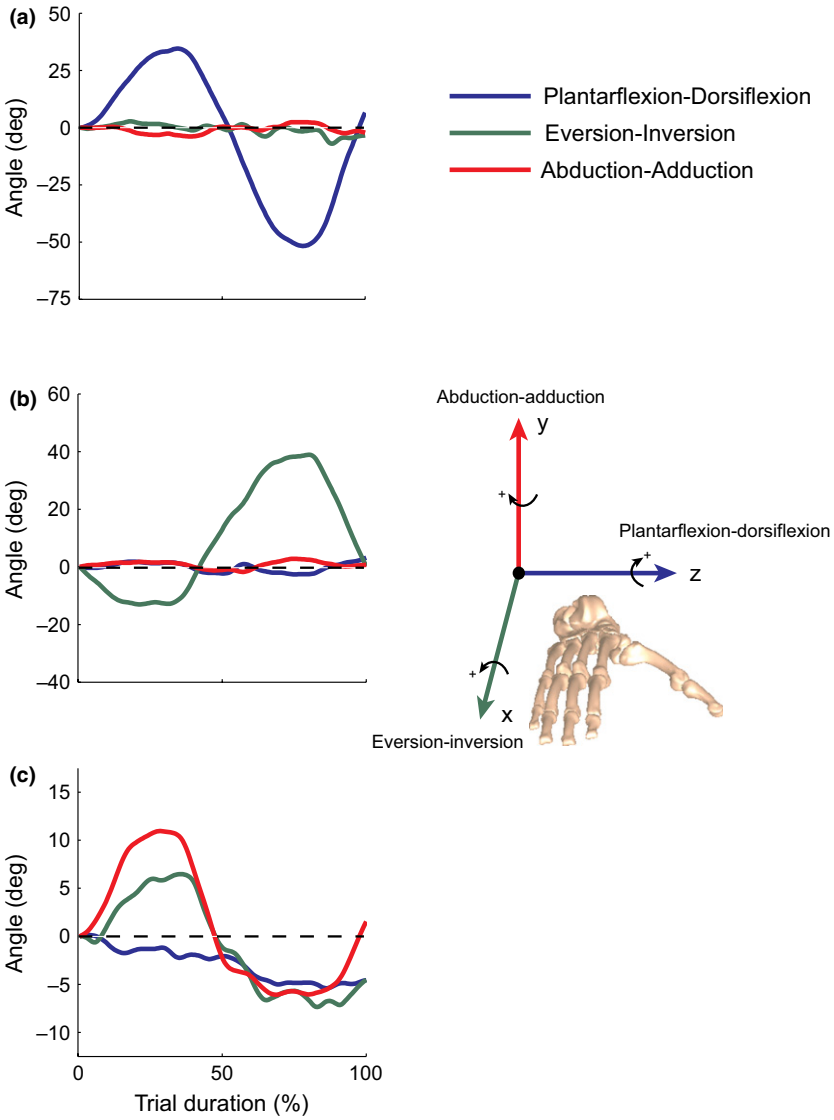

Fig. 2 Angular motion during representative (a) plantarflexion–dorsiflexion, (b) eversion–inversion and (c) abduction–adduction trials. Trial duration represents the percentage of time elapsed between the beginning of the trial (0) and the end of the trial (100). Each cycle of foot motion began and ended at neutral position (0°). Relatively large amounts of multi-plane motion occurred when the foot was abducted and adducted, whereas motion was restricted to a single plane when the foot was plantarflexed and dorsiflexed as well as everted and inverted.

internal tendon using a sharp scalpel. This approach exposes the proximal to distal paths of individual fascicles. We isolated three muscle fascicles (one per proximal, middle and distal regions of the muscle belly) and measured them using digital calipers (Fig. 3a). Care was taken to dissect out and identify the origin and insertion points of each fascicle prior to measurement; this ensured that the fascicle had not been damaged during the muscle bisection, and prevented underestimation of the actual *in vitro* fascicle length.

We determined both internal and external (surface) pennation angles for all MTUs. We calculated the internal pennation angle as a trigonometric function of fascicle length (L_f) and a fascicle height parameter (d). We measured height as the perpendicular distance from the plane of fascicle origin to the plane of distal fascicle insertion (Alexander & Vernon, 1975; Anapol & Barry, 1996; Fig. 3). From fascicle length and height, we calculated the internal pennation angle (α) as:

$$\alpha = \sin^{-1}(d/L_f) \quad (1)$$

We then measured the external (surface) pennation angle at the same three locations as close to the measured fascicle length as possible. For these measurements, we placed the muscle belly on a flat surface, and used a goniometer to determine the angle of the fascicle with respect to the distal muscle tendon (Eng et al. 2008; Ward et al. 2009). External pennation angles were measured to facilitate comparisons to those studies that have used this particular measurement (Carlson, 2006; Ward et al. 2009).

For each muscle, we used average fascicle length and internal pennation angle to calculate physiological cross-sectional area (PCSA; Lieber, 2010):

$$\text{PCSA} = (M_m \cdot \cos\alpha)/(L_f \cdot \rho) \quad (2)$$

where M_m is muscle mass (g), L_f is fascicle length (cm), and ρ is muscle density [1.0597 g cm^{-3} (Mendez & Keys, 1960)]. We selected internal pennation angle as the best representation of fascicle pennation for the purpose of PCSA calculation because of its

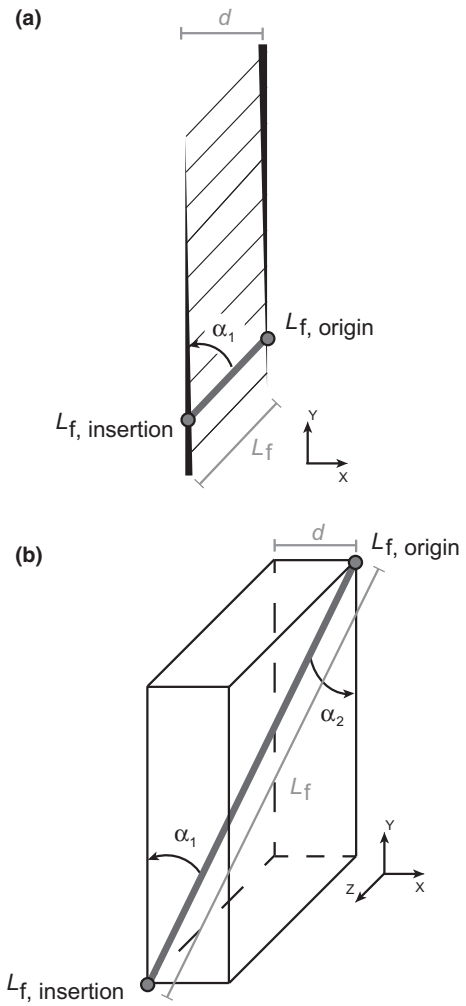

Fig. 3 Schematic of a sagittal section through a pennate muscle shown in (a) two dimensions and (b) three dimensions. L_f = length of muscle fascicle, d = perpendicular distance from plane of fascicle insertion to fascicle origin, and α = angle of pennation. The pennation angle was calculated as either internal pennation angle (α_1; X–Y plane) or external (surface) pennation angle (α_2; Y–Z plane).

relationship to the long axis of the muscle that shortens during contraction (Fig. 3b).

Comparative analyses

To account for differences in body size, we made comparisons among chimpanzee specimens and between humans and chimpanzees with dimensionless variables. We used foot length, measured as the distance from the posterior calcaneus to the tip of the third digit, to scale PF–DF moment arms; we used foot width, measured as the distance from the medial side of the head of the second metatarsal to the lateral side of the head of the fifth metatarsal, to scale EV–IN moment arms. We chose these metrics as moment arm scalars assuming that they are proportional to the maximum load arm lengths at the ankle and foot joints during similar movement tasks. This is the approach typically taken when comparing osteometric estimates of moment arm length within and between species (e.g. Schultz, 1963; Fleagle, 1976; Trinkaus, 1983; Strasser, 1992; Drapeau, 2004; Young, 2005), as it approximates the effective mechanical advantage (Biewener, 1989) at a joint.

We also compared the neutral position PF–DF moment arms that we calculated for chimpanzees with those presented by Spoor et al. (1990). To enable this comparison, we scaled the average neutral position moment arms reported in Spoor et al. (1990) by the average foot length of their specimens, then compared these values with the scaled neutral position values calculated in our own study. For this comparison, we calculated triceps surae moment arms for our specimens by averaging the values of the three superficial plantarflexors. We averaged all chimpanzee values between both specimens, except for m. peroneus brevis, for which a moment arm had only been determined for Chimp B.

For muscle architecture comparisons, we scaled muscle masses, fascicle lengths and PCSAs assuming geometric similarity within common chimpanzees. This approach has been taken in numerous previous ape muscle architecture studies (Thorpe et al. 1999; Payne et al. 2006a; Channon et al. 2009; but see also Myatt et al. 2011). Specifically, we scaled muscle masses by body mass (M_b) as $M_b^{1.0}$, fascicle length by $M_b^{0.33}$ and PCSAs by $M_b^{0.67}$, where M_b is in kg. For comparisons with Thorpe et al. (1999), Nagano (2001), Carlson (2006) and Myatt et al. (2011), we calculated PCSA with $\alpha = 0°$, because not all studies included measurements of pennation angles.

Results

PF–DF motion and moment arms

The chimpanzee ankle PF–DF range of motion was 105° in Chimp A and 91° in Chimp B (Table 3). The PF–DF moment arm curves for m. gastrocnemius medialis and lateralis at 0°, 45°, 90° and 135° of knee flexion are shown in Fig. 4, with equations for these curves given in Table 4. Unfortunately, due to recording problems, it was not possible to include the trial from Chimp A in which the knee was flexed at 135°. Mm. gastrocnemius lateralis and medialis moment arm curves show similar shapes and magnitudes at different knee flexion angles in both specimens, with moment arm lengths reaching peak values at 0–20° of ankle PF.

Moment arm curves for all MTUs during PF–DF are displayed in Fig. 5, with moment arm equations and model-fit statistics given in Tables 5 and 6, respectively. Under the criterion that MTU displacement vs. joint angle curves had $R^2 > 0.70$, PF–DF moment arm curves were derived for all MTUs in both specimens, with the exception of m. peroneus brevis in Chimp A. Generally, shape and magnitude of the PF–DF moment arm curves derived in both specimens are similar. Mm. gastrocnemius lateralis and medialis have the longest moment arms during PF, while m. extensor hallucis longus has the longest moment arm during most of DF. Most muscles (8 out of 10 in Chimp A; 7 out of 11 in Chimp B) show large ranges (i.e. > 1 cm) for moment arm lengths across PF–DF, suggesting that the mechanical advantage of these muscles changes considerably depending on ankle joint position. PF–DF moment arms tend to peak at 0–20° of

Table 3 Joint angle minimum (Min), maximum (Max) and range of motion (ROM = Max – Min) values in degrees.

	PF–DF			EV–IN		
	Max DF*	Max PF*	ROM	Max IN†	Max EV†	ROM
Chimp A	37.3	−68.1	105.4	49.1	−18.5	67.6
Chimp B	33.4	−57.2	90.6	39.3	−28.3	67.6
Mean	35.4	−62.7	98.1	44.2	−23.4	67.6

*Plantarflexion (PF) is negative and dorsiflexion (DF) is positive.
†Eversion (EV) is negative and inversion (IN) is positive.

PF; however, there is a notable exception to this trend: the deep plantarflexor moment arms tend to peak at maximum DF positions, while reaching their minima near neutral position (Fig. 5c,d).

EV–IN motion and moment arms

The chimpanzee ankle EV–IN range of motion was 68° in both Chimps A and B (Table 3). Moment arm curves for all muscles during EV–IN are displayed in Fig. 6, and moment arm equations and model-fit statistics are presented in Tables 7 and 8, respectively. Following the MTU displacement vs. joint angle $R^2 > 0.70$ criterion, EV–IN moment arms were derived for only a subset of the 11 available MTUs in Chimps A and B. Of these, EV–IN moment arm curves are similar in shape and magnitude between specimens for m. extensor hallucis longus, m. tibialis anterior and the peroneal muscles. M. peroneus longus and m. peroneus brevis have the longest EV moment arms, while m. tibialis anterior and m. extensor hallucis longus have the longest IN moment arms. The other muscles generally exhibit small EV–IN moment arms. For m. soleus, the between-specimen difference is notable; in Chimp A (Fig. 6a) m. soleus acts as an evertor, while in Chimp B (Fig. 6b) m. soleus acts as an invertor over the full range of joint motion. Moment arm ranges are large (> 1 cm) for all of the muscles of Chimp A, except m. flexor digitorum fibularis; Chimp B shows smaller moment arm ranges, with only m. extensor hallucis longus and the peroneal muscles possessing ranges > 1 cm. For both specimens, maximum EV–IN moment arm lengths tend to occur when the foot is positioned in 0–20° of IN, with some exceptions (e.g. soleus, deep plantarflexors).

Osteometric estimates of moment arms

Osteometric moment arm measurements of the superficial plantarflexors and the deep plantarflexors are shown in Fig. 7. Because osteometric estimates do not take into account the relative position of the limb segments when deriving moment arms, they should be most directly comparable to the tendon-excursion-based moment arms at neutral position. We compared the osteometric measurements to average values calculated from the neutral position moment arms of the superficial and deep plantarflexors. Average values were calculated because we did not have an *a priori* expectation as to the specific individual muscles within these groups to which the

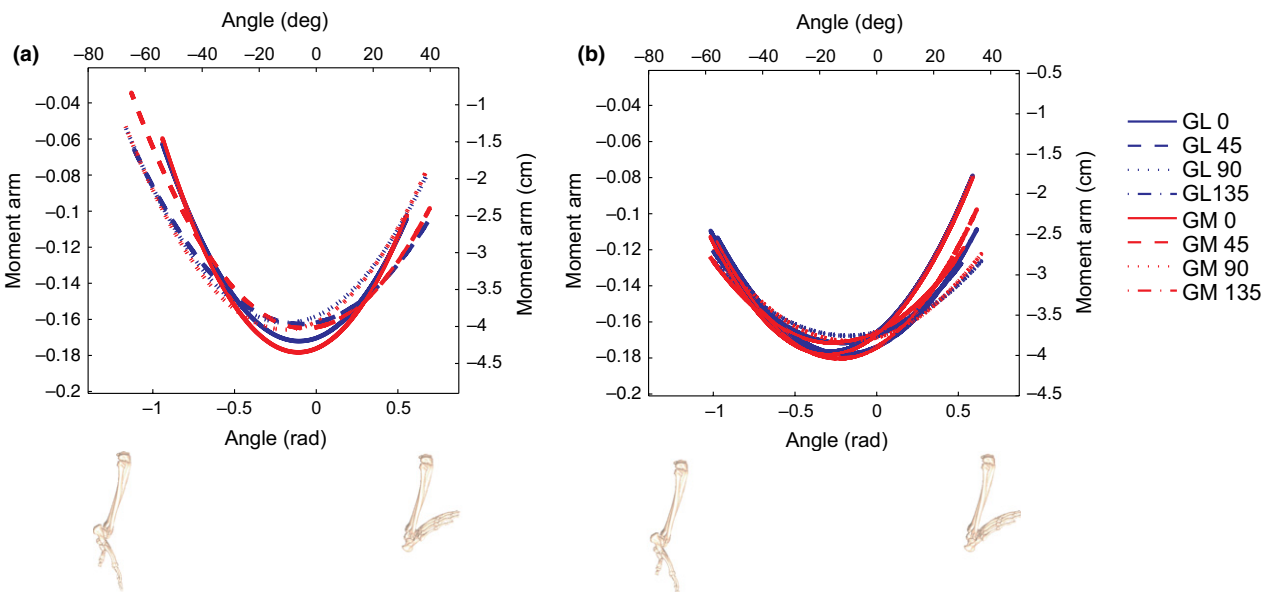

Fig. 4 Gastrocnemius moment arms during knee flexion. GL = m. gastrocnemius lateralis, GM = m. gastrocnemius medialis. The numbers following the muscle abbreviations in the legend denote the angle of knee flexion. (a) Chimp A moment arms; (b) Chimp B moment arms. Plantarflexion angles are negative and dorsiflexion angles are positive; negative moment arm values correspond to plantarflexion moment arms, and positive moment arm values correspond to dorsiflexion moment arms. Dimensional and dimensionless moment arm lengths appear on the right and left *y*-axes, respectively. Dimensionless values were calculated by dividing moment arm values by foot length.

Table 4 PF–DF moment arm equations for m. gastrocnemius medialis and lateralis at a range of knee flexion angles.

		Chimp A			Chimp B		
	Muscle	Moment arm eqn.	RMSE (cm)*	$R^{2\dagger}$	Moment arm eqn.	RMSE (cm)*	$R^{2\dagger}$
0°	GL	$y = -4.16 + 0.80x + 3.81x^2$	0.24	0.98	$y = -3.72 + 1.65x + 2.84x^2$	0.18	0.99
	GM	$y = -4.30 + 0.93x + 4.19x^2$	0.26	0.98	$y = -3.74 + 1.67x + 2.82x^2$	0.17	0.99
45°	GL	$y = -3.95 + 0.44x + 2.28x^2$	0.29	0.98	$y = -3.76 + 0.79x + 1.85x^2$	0.17	0.99
	GM	$y = -4.01 + 0.37x + 2.8x^2$	0.24	0.99	$y = -3.71 + 0.97x + 1.85x^2$	0.15	0.99
90°	GL	$y = -3.86 + 0.99x + 2.72x^2$	0.25	0.99	$y = -3.71 + 0.49x + 1.38x^2$	0.15	0.99
	GM	$y = -3.94 + 1.09x + 2.88x^2$	0.23	0.99	$y = -3.78 + 0.55x + 1.67x^2$	0.16	0.99
135°	GL	–	–	–	$y = -3.89 + 0.92x + 2.37x^2$	0.17	0.99
	GM	–	–	–	$y = -3.90 + 1.20x + 2.60x^2$	0.19	0.99

y = moment arm length (cm); x = joint angle (rad), where 0° joint angle is neutral position. Plantarflexion is negative and dorsiflexion is positive.

*Root mean square error (RMSE) calculated from ankle angle vs. MTU excursion least-squares regressions.

†Coefficient of determination (R^2) calculated from ankle angle vs. MTU excursion least-squares regressions.

GL, gastrocnemius lateralis; GM, gastrocnemius medialis.

osteometric dimensions should be compared. 'Calcaneal tuber length' (Chimp A: 4.20 cm; Chimp B: 3.97 cm) provides a much closer approximation of the average superficial plantarflexor moment arm values at neutral position (Chimp A: 4.01 cm; Chimp B: 3.62 cm) than does the 'pedal power arm' measurement (Chimp A: 3.19 cm; Chimp B: 2.70 cm). For the deep plantarflexors, the osteometric measurements (Chimp A: 1.40 cm; Chimp B: 1.25 cm) are slightly longer than the average moment arm values (Chimp A: 1.21 cm; Chimp B: 1.00 cm) calculated for these muscles.

Muscle architecture

Muscle masses and architecture measurements, including fascicle lengths, pennation angles and PCSAs, are reported in Table 9. The superficial plantarflexors make up the highest percentage of leg muscle mass in both specimens (A: 43.2%; B: 49.8%), followed by the deep plantarflexors (A: 27.3%; B: 21.3%), the dorsiflexors (A: 18.1%; B: 16.8%) and the peroneal muscles (A: 13.5%; B: 11.8%; Table 10). When normalized to body mass, all muscle groups are larger in Chimp A than in Chimp B.

Chimps A and B possess similar fascicle lengths ($\leq$ 2.5 cm difference), except in the cases of the mm. gastrocnemius lateralis and medialis, where Chimp B's fascicles are roughly twice the length of Chimp A's (Table 9). In both Chimps A and B, the dorsiflexors tend to have the longest fascicles, while m. tibialis posterior has the shortest fascicles. Internal and external pennation angles show similar trends in both specimens, with Chimp A exhibiting slightly larger pennation angles than Chimp B. The largest internal pennation angles are found in m. soleus for both specimens, whereas the smallest angles tend to be found in the dorsiflexors and deep plantarflexors. External pennation angles are notably larger (i.e. $>$ 10 °) than internal pennation angles for almost all muscles.

As with muscles masses, the greatest PCSAs belong to the superficial plantarflexors for both specimens, followed by the deep plantarflexors (Table 10). Unlike muscle masses, however, the dorsiflexors have the lowest PCSA values in both specimens. Chimp A possesses higher normalized combined PCSA values for all muscle groups compared with Chimp B, although this difference is very small for the peroneal muscles.

Discussion

PF–DF moment arms

Overall, PF–DF moment arms are similar between specimens, with dimensionless moment arm curves nearly identical in shape and magnitude for Chimps A and B for most MTUs. Minor exceptions to this observation occur with respect to small differences in magnitude and/or polynomial order between specimens for some of the deep plantarflexors, dorsiflexors and peroneal muscles. Of course, it is entirely expected that some moment arm variation will occur between individuals due to differences in MTU path and/or joint morphology, as has been previously documented in human studies (Spoor et al. 1990; Hintermann et al. 1994; Klein et al. 1996; McCullough et al. 2011) and two recent ape studies (Payne et al. 2006b; Channon et al. 2010). The PF–DF moment arms are mostly non-linear functions of ankle position, with many MTUs displaying appreciable moment arm length changes across joint angles. These changes indicate that ankle posture has a significant effect on moment production for the MTUs that act upon this joint. Knee joint angle has only a minor effect on moment arm lengths of the mm. gastrocnemii at the

ankle (Fig. 4). This finding indicates that changes in knee posture, such as those occurring when a chimpanzee switches from a quadrupedal to a bipedal locomotor mode (Jenkins, 1972; Sockol et al. 2007), have little influence on its PF moment arms.

Typically, MTUs display maximum PF–DF moment arms near neutral ankle positions, with moment arm lengths decreasing at greater joint angles. However, the moment arms of the deep plantarflexors exhibit the converse pattern of having their shortest lengths occurring near neutral position, and their greatest lengths near maximum PF and DF. Cineradiographs of PF–DF in Chimps A and B (unpublished data) suggest that additional subtalar joint motion during extreme PF and DF redirects the line of action of the deep plantarflexors. When the ankle approaches maximum DF, the talus appears to slide posteriorly, and as the ankle nears maximum PF, the talus slides anteriorly. Because the deep plantarflexors all run along the posterior surface of the talus, this unexpected motion likely explains the change in moment arms of these muscles without any noticeable effect on the superficial plantarflexors. Interestingly, several human studies have observed a similar but less pronounced pattern for the PF–DF moment arms of the deep plantarflexors (Spoor et al. 1990; McCullough et al. 2011), suggesting that some talar motion during PF–DF may not be unique to chimpanzees.

The moment arm lengths calculated for the superficial plantarflexors in this study are slightly different from those calculated by Thorpe et al. (1999) for triceps surae. Chimps A and B have longer moment arms in maximum PF and neutral position, but shorter moment arms in maximum DF than the specimen in Thorpe et al. (1999). This difference may be the result of different model-fitting approaches: for both Chimps A and B, moment arm lengths of the superficial plantarflexors change as non-linear functions of ankle position, in contrast to the linear function that Thorpe et al. (1999) determined to be the best fit to the data. The results herein are consistent with the expectation that a moment arm should change as a trigonometric function of joint angle (Delp & Loan, 1995; Pandy, 1999). It is likely then that the different results of our studies are due to a combination of different methodologies for deriving moment arm functions, as well as normal individual variation.

After non-dimensionalizing the PF–DF data using foot length, chimpanzees generally have shorter moment arms than humans (Table 11). This difference includes all of the leg musculature except m. flexor digitorum tibalis and m. tibialis posterior, which are similar between species. The larger PF moment arms in humans may reflect a greater reliance of bipedal hominins on ankle force and work output compared with chimpanzees, which, in contrast, generate their largest joint moments at the hip in quadrupedalism and bipedalism (Sockol et al. 2007).

EV–IN moment arms

As with PF–DF, most MTUs exhibit EV–IN moment arm functions that are non-linear with respect to changes in ankle position, as well as large EV–IN moment arm length ranges. Again, these results indicate different ankle moment production capabilities depending on joint posture. The normalized EV–IN moment arm curves that were calculated for muscles whose lines of action pass relatively far from the joint axis of rotation (i.e. m. extensor hallucis longus, m. tibialis anterior, peroneal muscles) show very similar shapes and magnitudes in our two specimens. However, the superficial plantarflexors exhibit EV moment arms in Chimp A, while m. soleus has a small IN moment arm in Chimp B. This discrepancy could be explained by minor differences in the transverse tarsal and/or subtalar joint axes in these specimens, which would result in slightly different composite EV–IN axes of rotation. However, the short lengths of these moment arms in both specimens suggest that, in both cases, the axis about which pure EV–IN occurs in the chimpanzee foot is positioned close to the long axis of the calcaneus. This finding is consistent with human studies that used similar methods to measure EV–IN moment arms. These studies have reported that the superficial plantarflexors can act as both evertors and invertors, depending on foot posture (Klein et al. 1996; McCullough et al. 2011).

Joint ranges of motion

The total PF–DF range of motion was higher in Chimp A than Chimp B, with an average value of 98° for the two specimens. These values are close to the cadaveric measurements of Thorpe et al. (1999) and Nagano (2001), who found ~ 100° and 88° total ranges of motion in their specimens, respectively. In spite of the intraspecific variation in chimpanzees, these values are still much higher than those reported from *in vivo* (Boone & Azen, 1979; Grimston et al.

Fig. 5 Plantarflexion–dorsiflexion moment arms. (a) Chimp A superficial plantarflexors; (b) Chimp B superficial plantarflexors; (c) Chimp A deep plantarflexors; (d) Chimp B deep plantarflexors; (e) Chimp A peroneals; (f) Chimp B peroneals; (g) Chimp A dorsiflexors; (h) Chimp B dorsiflexors. See Table 2 for muscle abbreviations. GM and GL data were from trials where knee flexion angle was 0°. Plantarflexion angles are negative, and dorsiflexion angles are positive. Negative moment arm values correspond to plantarflexion moment arms, and positive moment arm values correspond to dorsiflexion moment arms. Dimensional and dimensionless moment arm lengths appear on the right and left *y*-axes, respectively. Dimensionless values were calculated by dividing moment arm values by foot length.

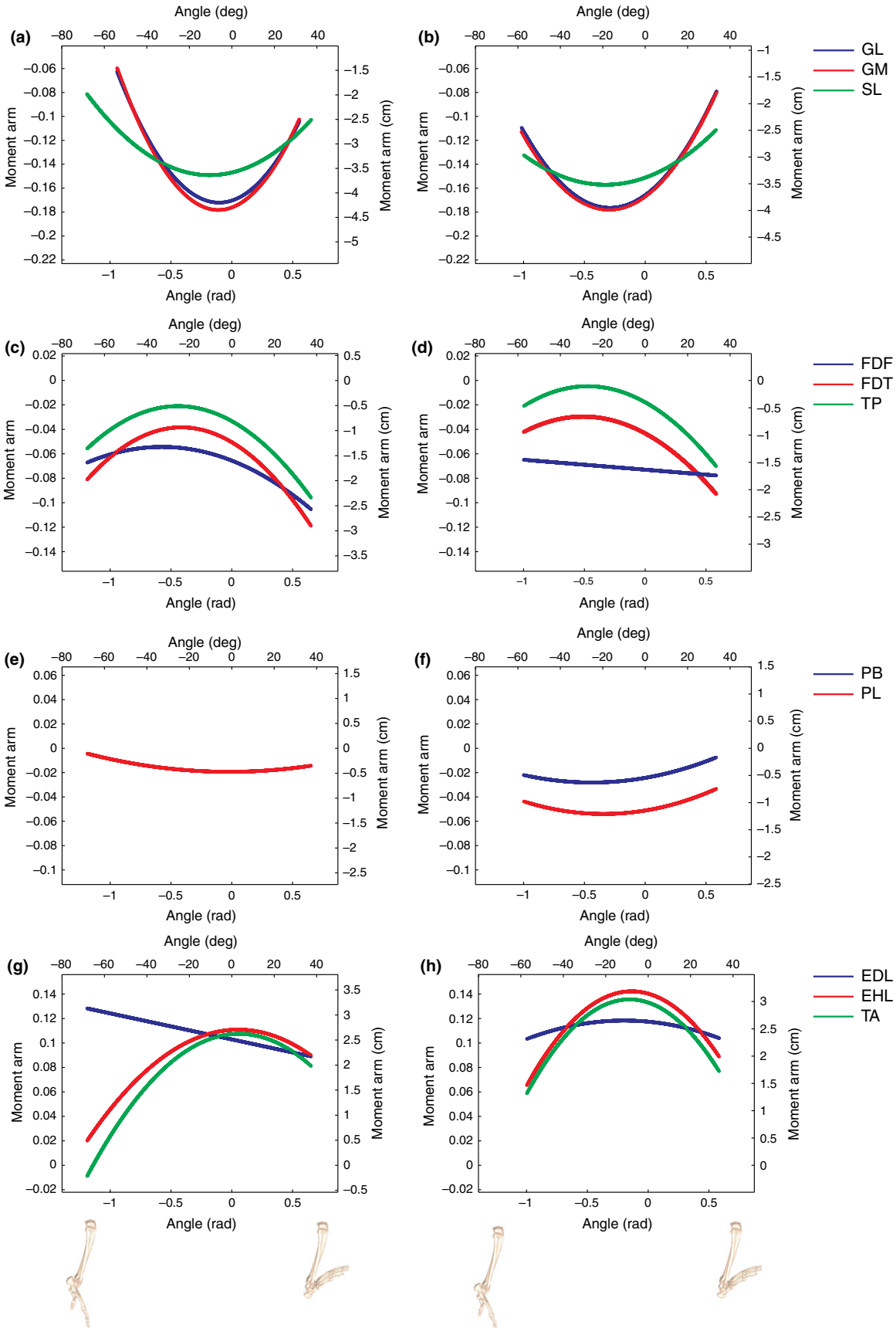

Table 5 Moment arm equations for muscles during PF–DF.

	Chimp A			Chimp B		
Muscle	Moment arm eqn	RMSE (cm)*	$R^{2\dagger}$	Moment arm eqn.	RMSE (cm)*	$R^{2\dagger}$
EDL	$y = 2.51 - 0.52x$	0.19	0.99	$y = 2.63 - 0.21x - 0.53x^2$	0.65	0.99
EHL	$y = 2.70 - 0.15x - 1.44x^2$	0.26	0.97	$y = 3.14 - 0.63x - 2.31x^2$	0.18	0.97
FDF	$y = -1.60 - 0.95x - 0.83x^2$	0.14	0.98	$y = -0.97 - 1.21x - 1.18x^2$	0.16	0.92
FDT	$y = -1.23 - 1.43x - 1.73x^2$	0.19	0.95	$y = -1.63 - 0.18x$	0.11	0.98
GL	$y = -4.16 + 0.80x + 3.81x^2$	0.24	0.98	$y = -3.72 + 1.65x + 2.84x^2$	0.18	0.99
GM	$y = -4.30 + 0.93x + 4.19x^2$	0.26	0.98	$y = -3.74 + 1.67x + 2.82x^2$	0.17	0.99
PB	–	0.09	0.47	$y = -0.54 + 0.39x + 0.54x^2$	0.15	0.79
PL	$y = -0.47 + 0.01x + 0.27x^2$	0.09	0.88	$y = -1.15 + 0.37x + 0.54x^2$	0.16	0.94
SL	$y = -3.58 + 0.59x + 1.63x^2$	0.15	0.99	$y = -3.39 + 0.81x + 1.23x^2$	0.15	0.99
TA	$y = 2.62 + 0.22x - 1.82x^2$	0.11	0.99	$y = 2.98 - 0.75x - 2.42x^2$	0.14	0.99
TP	$y = -0.81 - 1.34x - 1.52x^2$	0.18	0.90	$y = -0.40 - 1.24x - 1.31x^2$	0.11	0.81

y = moment arm length (cm); x = joint angle (rad), where 0 radians is neutral position. Plantarflexion is negative and dorsiflexion is positive.

*Root mean square error (RMSE) calculated from ankle angle vs. MTU excursion least-squares regressions.

†Coefficient of determination (R^2) calculated from ankle angle vs. MTU excursion least-squares regressions.

EDL, extensor digitorum longus; EHL, extensor hallucis longus; FDF, flexor digitorum fibularis; FDT, flexor digitorum tibialis; GL, gastrocnemius lateralis; GM, gastrocnemius medialis; PB, peroneus brevis; PL, peroneus longus; SL, soleus; TA, tibialis anterior; TP, tibialis posterior.

Table 6 Statistics for PF–DF moment arms.

	Chimp A				Chimp B			
Muscle	Neutral moment arm (cm)*	Dimensionless moment arm†	Range (cm)‡		Neutral moment arm (cm)*	Dimensionless moment arm†	Range (cm)‡	
EDL	2.51	0.10	2.17	3.13	2.63	0.12	2.31	2.65
EHL	2.70	0.11	0.50	2.71	3.14	0.14	1.47	3.19
FDF	−1.60	−0.07	−1.33	−2.57	−0.97	−0.04	−0.66	−2.08
FDT	−1.23	−0.05	−0.94	−2.9	−1.63	−0.07	−1.45	−1.74
GL	−4.16	−0.17	−1.53	−4.20	−3.72	−0.17	−1.76	−3.95
GM	−4.30	−0.18	−1.46	−4.35	−3.74	−0.17	−1.79	−3.99
PB	–	–	–	–	−0.54	−0.02	−0.17	−0.63
PL	−0.47	−0.02	−0.10	−0.47	−1.15	−0.05	−0.75	−1.21
SL	−3.58	−0.15	−1.99	−3.64	−3.39	−0.15	−2.49	−3.52
TA	2.62	0.11	−0.21	2.62	2.98	0.13	1.28	3.04
TP	−0.81	−0.03	−0.52	−2.34	−0.40	−0.02	−0.10	−1.57

*Calculated when the foot is in neutral position. Plantarflexion is negative and dorsiflexion is positive.

†Neutral position moment arm divided by foot width. Plantarflexion is negative and dorsiflexion is positive.

‡Values in the left and right columns represent the shortest and longest moment arms across the range of joint motion, respectively.

EDL, extensor digitorum longus; EHL, extensor hallucis longus; FDF, flexor digitorum fibularis; FDT, flexor digitorum tibialis; GL, gastrocnemius lateralis; GM, gastrocnemius medialis; PB, peroneus brevis; PL, peroneus longus; SL, soleus; TA, tibialis anterior; TP, tibialis posterior.

1993; 60–71°) or *in vitro* (Siegler et al. 1988; 66°) human range of motion studies. These finding are consistent with previous comparative studies of the talocrural joint (Stern & Susman, 1983; Susman et al. 1984; Latimer et al. 1987), which indicate that chimpanzees possess larger ranges of motion in PF–DF than humans, on average. Several skeletal correlates of this substantial range of motion have been proposed, including the larger talar trochlea articular surface area (Stern & Susman, 1983; Susman et al. 1984; Latimer et al. 1987), and an oblique orientation of the distal fibular facet (Stern & Susman, 1983; Susman et al. 1984).

In both Chimps A and B, the total EV–IN range of motion was 68°, which is considerably larger than *in vivo* (Grimston et al. 1993; 29–41°) or *in vitro* (Siegler et al. 1988; 32°)

Table 7 Moment arm equations for muscles during EV–IN.

	Chimp A			Chimp B		
Muscle	Moment arm eqn.	RMSE (cm)*	$R^{2\dagger}$	Moment arm eqn.	RMSE (cm)*	$R^{2\dagger}$
EDL	–	0.23	0.33	$y = -0.64 - 1.08x + 1.67x^2$	0.72	0.81
EHL	$y = 1.43 - 0.94x - 1.55x^2$	0.21	0.85	$y = 1.52 + 0.32x - 3.10x^2$	0.14	0.91
FDF	$y = -0.30 - 0.69x - 0.39x^2$	0.08	0.81	–	0.06	0.29
FDT	–	0.15	0.35	$y = 0.47 - 0.32x - 0.51x^2$	0.07	0.77
GL	$y = -1.08 - 1.99x + 3.54x^2$	0.09	0.80	–	0.19	0.46
GM	$y = -0.43 - 1.16x$	0.11	0.91	–	0.20	0.47
PB	$y = -1.94 - 2.79x + 5.57x^2$	0.29	0.85	$y = -1.49 - 3.06x + 4.27x^2$	0.15	0.95
PL	$y = -2.18 - 1.00x + 3.55x^2$	0.30	0.87	$y = -1.80 - 2.02x + 3.68x^2$	0.12	0.97
SL	$y = -0.12 - 0.62x + 2.97x^2$	0.12	0.73	$y = 0.45 - 0.65x$	0.08	0.71
TA	$y = 1.63 + 0.57x - 4.22x^2$	0.21	0.86	$y = 1.15 + 0.51x - 1.89x^2$	0.12	0.92
TP	–	0.14	0.61	$y = 0.55 - 0.18x$	0.10	0.81

y = moment arm length (cm); x = joint angle (rad), where 0 radians is neutral position. Eversion is negative and inversion is positive.
*Root mean square error (RMSE) calculated from ankle angle vs. MTU excursion least-squares regressions.
†Coefficient of determination (R^2) calculated from ankle angle vs. MTU excursion least-squares regressions.
EDL, extensor digitorum longus; EHL, extensor hallucis longus; FDF, flexor digitorum fibularis; FDT, flexor digitorum tibialis; GL, gastrocnemius lateralis; GM, gastrocnemius medialis; PB, peroneus brevis; PL, peroneus longus; SL, soleus; TA, tibialis anterior; TP, tibialis posterior.

Table 8 Statistics for EV–IN moment arms at neutral position.

	Chimp A				Chimp B			
Muscle	Neutral moment arm (cm)*	Dimensionless moment arm†	Range (cm)‡		Neutral moment arm (cm)*	Dimensionless moment arm†	Range (cm)‡	
EDL	–	–	–	–	−0.64	−0.12	0.12	0.82
EHL	1.43	0.23	−0.05	−1.57	1.52	0.29	−0.48	−1.53
FDF	−0.30	−0.05	0.05	0.95	–	–	–	–
FDT	–	–	–	–	−0.47	−0.09	−0.17	−0.53
GL	−1.08	−0.18	−0.67	1.36	–	–	–	–
GM	−0.43	−0.07	−0.12	1.07	–	–	–	–
PB	−1.94	−0.32	−0.79	2.29	−1.49	−0.28	0.07	2.04
PL	−2.18	−0.36	0.83	2.25	−1.80	−0.34	0.77	2.08
SL	−0.12	−0.02	0.09	1.95	0.45	0.08	0.7	0.77
TA	1.63	0.27	−0.03	−1.65	1.15	0.22	−0.21	−1.19
TP	–	–	–	–	0.55	0.10	−0.13	−0.36

*Calculated when the foot is in neutral position. Inversion is negative and eversion is positive.
†Neutral position moment arm divided by foot width. Inversion is negative and eversion is positive.
‡Values in the left and right columns represent the shortest and longest moment arms across the range of joint motion, respectively.
EDL, extensor digitorum longus; EHL, extensor hallucis longus; FDF, flexor digitorum fibularis; FDT, flexor digitorum tibialis; GL, gastrocnemius lateralis; GM, gastrocnemius medialis; PB, peroneus brevis; PL, peroneus longus; SL, soleus; TA, tibialis anterior; TP, tibialis posterior.

human measurements. This raises the question of which anatomical elements facilitate the larger EV–IN range of motion found in chimpanzees. Differences in plantar ligaments and soft tissue structures appear to allow greater laxity in the chimpanzee midtarsal joints (Lewis, 1980b; Susman, 1983; Gomberg, 1985). Additionally, studies of tarsal morphology have both observed (Elftman & Manter, 1935b; Bojsen-Møller, 1979; Lewis, 1980b) and measured distinct differences in overall shape (Kidd et al. 1996; Jungers et al. 2009) and curvature (Deloison, 1985; Latimer & Lovejoy, 1989; Sarmiento & Marcus, 2000; Gebo & Schwartz, 2006) of the subtalar, talonavicular and calcaneocuboid joint articu-

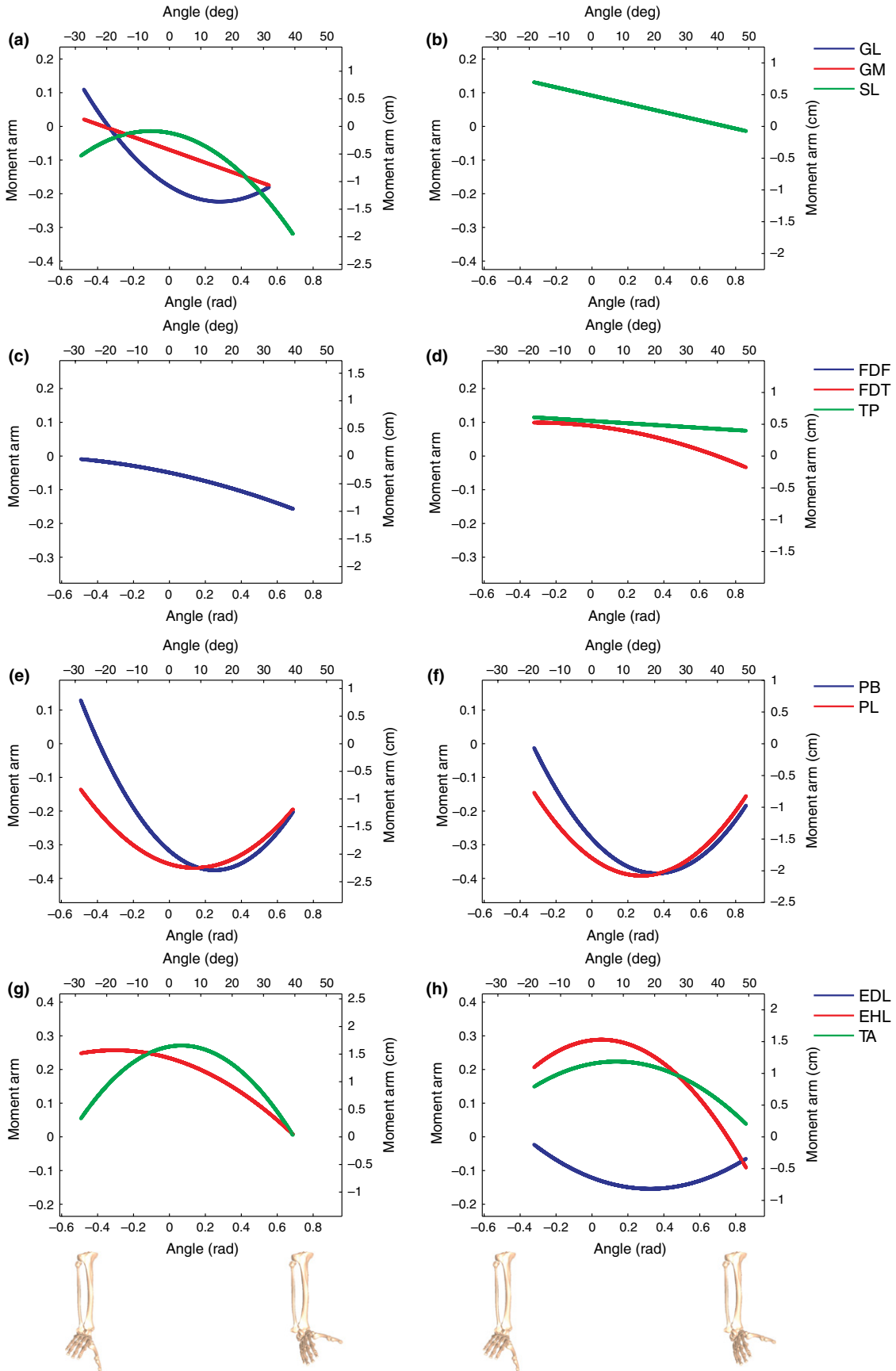

Fig. 6 Eversion–inversion moment arms. (a) Chimp A superficial plantarflexors; (b) Chimp B superficial plantarflexors; (c) Chimp A deep plantarflexors; (d) Chimp B deep plantarflexors; (e) Chimp A peroneals; (f) Chimp B peroneals; (g) Chimp A dorsiflexors; (h) Chimp B dorsiflexors. See Table 2 for muscle abbreviations. GM and GL data were from trials where knee flexion angle was 0°. Eversion angles are negative, and inversion angles are positive. Negative moment arm values correspond to eversion moment arms, and positive moment arm values correspond to inversion moment arms. Dimensional and dimensionless moment arm lengths appear on the right and left *y*-axes, respectively. Dimensionless values were calculated by dividing moment arm values by foot width.

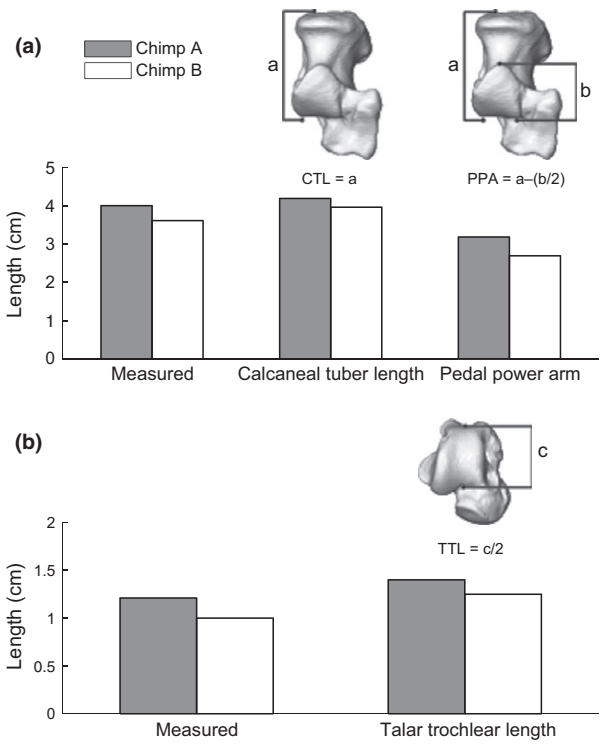

Fig. 7 Osteometric estimates of moment arm lengths (cm). (a) Average tendon-excursion measurement of GL, GM and SL moment arm lengths compared with 'calcaneal tuber length' (CTL) and 'pedal power arm' (PPA) osteometrics. (b) Average tendon-excursion measurements of TP, FDF and FDT moment arm lengths compared with one-half talar trochlear length (TTL).

lar surfaces in chimpanzees and humans. Because EV–IN likely occurs about the subtalar and transverse tarsal joints, the size and shape of the participating skeletal elements may be more important than the orientation of the talar trochlea in understanding the evolution of hominin foot EV–IN capabilities, which has been the focus of some previous studies of foot IN (Latimer et al. 1987; DeSilva, 2009). Nevertheless, additional data on the motion of the chimpanzee and human foot skeleton during EV–IN are needed to identify robust skeletal correlates of joint mobility.

Osteometric estimates of moment arms

In chimpanzees, 'calcaneal tuber length' (Raichlen et al. 2011) provides a closer approximation of the actual moment arm of the superficial plantarflexors than does the 'pedal power arm' (Schultz, 1963; Strasser, 1992). *A priori* the 'pedal power arm' might be expected to provide a more accurate estimate, because its multi-measurement derivation attempts to take into account the position of the talocrural joint axis of rotation by using the midpoint of the posterior subtalar joint surface as its distal limit. However, our results suggest that in practice this adjustment leads to an underestimation of the actual moment arm length, presumably because the actual talocrural joint axis of rotation is located further anteriorly than this metric assumes. Additional studies of other taxa are needed to fully evaluate the ubiquity of these findings for estimating superficial plantarflexor moment arms across species. Nevertheless, these results confirm that an osteometric approximation of the superficial plantarflexor moment arm length at neutral position can be obtained in chimpanzees, and suggests that this metric may be useful for comparative studies of hominin fossil remains.

Half talar trochlear length provides a reasonable approximation of deep plantarflexor moment arm length, albeit a slight overestimate. This overestimation could be due to the effect of averaging the moment arms of all three deep plantarflexors to calculate a single value, given the non-coincident position of the tendons where they cross the talocrural joint. Or, the PF–DF axis of rotation could be positioned slightly posterior to the middle of the talar trochlea at neutral position. Our osteometric measurement is based upon the location of the groove for the tendon of m. flexor digitorum fibularis; however, moment arm data from this study suggest that the tendons of m. tibialis posterior and m. flexor digitorum tibialis pass slightly closer to the talocrural joint axis of rotation.

Leg muscle architecture

The data presented herein expand the number of individuals for which muscle mass and architectural variables have been measured in chimpanzees. In dimensionless form, the muscle mass data from Chimps A and B are similar to measurements from Thorpe et al. (1999), Nagano (2001) and Myatt et al. (2011; Table 10), but with Chimp B falling at the lower end of this range. One potential contributor to variation among specimens in dimensionless measurements is differences in percentage body fat. For example, the body mass of Chimp B is quite large for a wild, adult female chimpanzee (Smith & Jungers, 1997; but see Sockol et al. 2007), and it is possible that this individual had a higher percentage of body fat at time of death than other specimens. In

Table 9 Muscle architecture measurements.

	Chimp A					Chimp B				
Muscle	Mass (g)	Fascicle length (cm)	Internal pennation angle (°)	External pennation angle (°)	PCSA (cm^2)	Mass (g)	Fascicle length (cm)	Internal pennation angle (°)	External pennation angle (°)	PCSA (cm^2)
EDL	46	13.2 ± 0.1	2 ± 1	0	3.3	48	10.7 ± 0.6	4 ± 1	15 ± 1	4.2
EHL	17	11.4 ± 1.0	0	0	1.4	18	10.9 ± 0.4	0	9 ± 3	1.6
FDF	127	6.0 ± 0.6	11 ± 3	17 ± 9	19.5	96	8.4 ± 0.4	5 ± 1	20 ± 10	10.7
FDT	47	5.4 ± 0.3	8 ± 2	35 ± 14	8.1	37	6.6 ± 0.3	6 ± 2	27 ± 7	5.3
GL	122	4.9 ± 0.6	19 ± 3	34 ± 6	22.4	81	9.0 ± 0.5	4 ± 1	21 ± 3	8.5
GM	123	4.0 ± 0.8	14 ± 6	34 ± 13	28.0	140	9.2 ± 0.3	7 ± 1	23 ± 9	14.2
PB	33	4.8 ± 0.1	8 ± 1	21 ± 10	6.5	38	5.0 ± 0.6	9 ± 2	17 ± 4	7.1
PL	83	5.9 ± 0.6	10 ± 4	19 ± 5	13.1	78	5.2 ± 0.4	14 ± 3	20 ± 6	13.7
SL	188	3.1 ± 0.6	29 ± 6	46 ± 6	49.6	256	5.4 ± 0.2	19 ± 2	32 ± 9	42.1
TA*	118	8.5 ± 0.4	6 ± 1	19 ± 2	13.1	95	8.9 ± 0.6	8 ± 2	18 ± 6	9.9
TP	100	2.3 ± 0.2	15 ± 4	41 ± 11	39.0	71	4.1 ± 0.3	12 ± 2	22 ± 2	16.0

*Chimpanzees possess a second head of m. tibialis anterior, sometimes referred to as m. abductor hallucis longus (Aiello & Dean, 1990), with a similar insertion and path as the main head of m. tibialis anterior. Fascicle lengths and pennation angles were measured separately for each of the two heads, and then averaged.
EDL, extensor digitorum longus; EHL, extensor hallucis longus; FDF, flexor digitorum fibularis; FDT, flexor digitorum tibialis; GL, gastrocnemius lateralis; GM, gastrocnemius medialis; PB, peroneus brevis; PCSA, physiological cross-sectional area; PL, peroneus longus; SL, soleus; TA, tibialis anterior; TP, tibialis posterior.

Table 10 Dimensionless muscle masses, fascicle lengths and PCSAs of six chimpanzees.

Muscle groups		Chimp A	Chimp B	Thorpe et al.	Nagano	Carlson	Myatt et al.
GM, GL, SL*	M_m	6.8	5.9	7.7	5.9	2.4	6.5
TP, FDF, FDT*	M_m	4.3	2.5	5.1	4.2	1.3	4.7
TA, EHL, EDL*	M_m	2.9	2.0	2.5	2.9	1.3	3.8
PL, PB*	M_m	1.8	1.4	2.0	1.9	0.6	1.9
GM, GL, SL†	L_f	1.0	1.7	2.1	2.5	0.9	1.5
TP, FDF, FDT†	L_f	1.2	1.5	1.5	2.4	1.3	1.2
TA, EHL, EDL†	L_f	2.5	2.3	3.2	2.9	2.4	2.2
PL, PB†	L_f	1.4	1.2	1.6	1.4	1.4	1.6
GM, GL, SL‡	PCSA	6.8	3.5	3.6	2.3	2.6	4.6
TP, FDF, FDT‡	PCSA	4.3	1.7	3.9	1.7	1.2	4.6
TA, EHL, EDL‡	PCSA	1.1	0.8	0.7	0.9	0.5	1.7
PL, PB‡	PCSA	1.2	1.1	1.2	1.2	0.4	1.1

*Calculated as: $\Sigma M_m / M_b^{1.0}$.
†Calculated as: $[\Sigma(L_f \cdot M_m)/\Sigma M_m]/M_b^{0.33}$.
‡Calculated as: $\Sigma PCSA / M_b^{0.67}$.
EDL, extensor digitorum longus; EHL, extensor hallucis longus; FDF, flexor digitorum fibularis; FDT, flexor digitorum tibialis; GL, gastrocnemius lateralis; GM, gastrocnemius medialis; PB, peroneus brevis; PCSA, physiological cross-sectional area; PL, peroneus longus; SL, soleus; TA, tibialis anterior; TP, tibialis posterior.

this case, the dimensionless metrics for Chimp B would be artificially deflated by factors of [body fat mass]$^{0.33-1.0}$ when compared with chimpanzees with a much lower percentage of body fat. That is, the denominator used to scale architectural variables would be smaller for this specimen if only lean mass was used to calculate dimensionless metrics. This may account for some of the differences between Chimps A and B in dimensionless metrics, especially muscle mass. It is also notable that individual 2 in Carlson (2006) is lower than other studies, with dimensionless masses that are about half those of other specimens. This may be due to individual variation, illness and/or the effects of post mortem tissue preservation, as noted in Carlson (2006). Clearly, more data on chimpanzee muscle mass and architecture are needed to provide a robust context for the current range of variation observed in these parameters.

The dimensionless muscle fascicle lengths of Chimps A and B are also within the measurement ranges of Thorpe

Table 11 Scaled average PF–DF moment arms for humans and chimpanzees at neutral position.

	Human*	Chimpanzee†
EDL	0.13	0.11 ± 0.01
EHL	0.18	0.13 ± 0.02
FDF	−0.10	−0.06 ± 0.02
FDT	−0.05	−0.06 ± 0.01
PB	−0.05	−0.02
PL	−0.05	−0.03 ± 0.02
TA	0.16	0.12 ± 0.02
TP	−0.03	−0.03 ± 0.01
GM, GL, SL‡	−0.20	−0.16 ± 0.01

*From Spoor et al. (1990), scaled using the average foot length of 26.05 cm.
†Scaled by foot length for Chimps A and B (see Table 1).
‡Average of GM, GL and SL moment arm lengths.
EDL, extensor digitorum longus; EHL, extensor hallucis longus; FDF, flexor digitorum fibularis; FDT, flexor digitorum tibialis; GL, gastrocnemius lateralis; GM, gastrocnemius medialis; PB, peroneus brevis; PL, peroneus longus; SL, soleus; TA, tibialis anterior; TP, tibialis posterior.

et al. (1999), Nagano (2001), Carlson (2006) and Myatt et al. (2011; Table 10). In our study and others, the dorsiflexors have the longest muscle fascicle lengths. However, it should be noted that for the fascicles of m. gastrocnemius, there is substantial variation between the two individuals measured here. The fascicles of mm. gastrocnemius medialis and lateralis were almost twice as long in Chimp B than in Chimp A, and discrepancies of similar magnitude occur between specimens from other studies. There are several possible explanations for the substantial intraspecific variation observed in chimpanzees, not the least of which is the inherent difficulty of obtaining robust, representative measurements of average fascicle lengths per muscle. In future studies, the chemical digestion of muscle connective tissues prior to fascicle length measurements (Perry & Wall, 2008; Perry et al. 2011) may reduce random error associated with undersampling, because this approach permits much larger numbers of fascicles to be easily isolated and measured per unit time. An additional source of error may be that none of the chimpanzee muscle fascicle length measurements collected to date has been corrected to optimal resting length (Lieber et al. 1997; Ward et al. 2009). The use of sarcomere-length-adjusted metrics should reduce the random variance between subjects, and help to clarify intraspecific scaling patterns of this trait. Of course, other physiological factors such as activity patterns, age and sex may also play a role.

Finally, it is well known that muscle fascicle pennation angles have only a modest effect on calculations of PCSA, because the magnitude of this effect is equal to the cosine of the angle (see Eq. 2). Our results (when internal pennation angle is used) generally confirm the findings of previous chimpanzee studies (Nagano, 2001; Carlson, 2006), that the majority of leg muscles possess pennation angles $< 20°$. Therefore, pennation angle is not likely to have a major influence on muscle force production at the ankle and foot joints in chimpanzees (Zajac, 1989). However, we believe that pennation angle is still an important measurement in chimpanzee limb muscle architecture studies, because in certain muscles (e.g. m. soleus) it will have a noticeable effect on PCSA calculation.

Conclusions

The main goal of this study was to determine the effect of chimpanzee knee and ankle joint position on the three-dimensional moment arms of the MTUs of the leg, as well as provide new measurements of ankle and foot ranges of motion. Our results indicate that moment arm lengths change substantially across the range of motion allowed at the chimpanzee ankle and foot joints, but are not significantly affected by knee position. Electromyography data of chimpanzee leg muscle activation patterns are needed to evaluate the extent to which the shorter moment arms observed at greater joint excursion angles influence the work requirements of these muscles during locomotion. In agreement with Payne et al.'s (2006b) study of moment arms in other ape species, chimpanzees possess relatively smaller moment arms at the ankle than modern humans, but are capable of muscle force and moment-generation over a wider range of leg and foot positions. Joint kinematic studies report that chimpanzee and bonobo ankles operate in the range of about $-40°$ to $45°$ PF–DF during overground walking and vertical climbing (Jenkins, 1972; D'Aout et al. 2002; DeSilva, 2009), while the operating ranges for EV–IN are unknown. This is consistent with the more arboreal locomotor repertoire of chimpanzees and the general hypothesis that the human ankle and foot have become less mobile for terrestrial bipedalism (Elftman & Manter, 1935b; Bojsen-Møller, 1979; Susman, 1983). In the future, the moment arm data presented here can be compared with those collected from other ape taxa (Payne et al. 2006b; Channon et al. 2010) to achieve a broader understanding of how ankle and foot musculoskeletal geometry has evolved to enable the different locomotor repertoires exhibited by these species.

The lengths of the superficial and deep plantarflexors at neutral position are well predicted by 'calcaneal tuber length' (Raichlen et al. 2011) and half talar trochlear length, respectively, for the two specimens in this study. These results provide support for the use of these metrics as simple surrogates of MTU moment arms in comparative analyses. Tracking the evolution of these traits in the fossil record may provide new insights into the evolution of hominin ankle function and locomotor performance capabilities.

The mass and architecture of chimpanzee leg musculature are similar to those previously published, but increase the body size range over which chimpanzee leg muscle data

have been collected. These data will be useful for future comparative studies of ape muscle metrics, especially those aimed at clarifying intra- and interspecific variation and size-scaling patterns (c.f. Payne et al. 2006a; Myatt et al. 2011), as well as improving dynamic estimates of muscle force requirements in musculoskeletal model-based studies of locomotion.

Acknowledgements

The authors thank B. Demes and S. Larson for the use of their chimpanzee hind limb specimens, and A. Nagano for sharing his chimpanzee hind limb muscle dataset. B. Demes, W. Jungers, S. Larson and R. Susman provided many helpful comments on earlier versions of the manuscript. Thanks also to two anonymous reviewers for their helpful comments. This study was supported by the National Science Foundation (BCS 0935321).

Author contributions

N. B. H. and M. C. O. designed the research, collected and analyzed the data, and wrote the manuscript.

References

Aiello LC, Dean MC (1990) *An Introduction to Human Evolutionary Anatomy*. London: Academic Press.

Akaike H (1974) A new look at statistical model identification. *IEEE Trans Automat Contr* **19**, 716–723.

Alexander RM, Vernon A (1975) The dimensions of the knee and ankle muscles and the forces they exert. *J Hum Mov Stud* **1**, 115–123.

An KN, Ueba Y, Chao EY, et al. (1983) Tendon excursion and moment arm of index finger muscles. *J Biomech* **16**, 419–425.

An KN, Takahashi K, Harrigan TP, et al. (1984) Determination of muscle orientations and moment arms. *J Biomech Eng* **106**, 280–282.

Anapol F, Barry K (1996) Fiber architecture of the extensors of the hindlimb in semiterrestrial and arboreal guenons. *Am J Phys Anthropol* **99**, 429–447.

Biewener AA (1989) Scaling body support in mammals: limb posture and muscle mechanics. *Science* **245**, 45–48.

Bojsen-Møller F (1979) Calcaneocuboid joint and stability of the longitudinal arch of the foot at high and low gear push off. *J Anat* **129**, 165–176.

Boone DC, Azen SP (1979) Normal range of motion of joints in male subjects. *J Bone Joint Surg* **61**, 756–759.

Brand PW, Cranor KC, Ellis JC (1975) Tendon and pulleys at the metacarpo-phalangeal joint of a finger. *J Bone Joint Surg* **57**, 779–784.

Carlson KJ (2006) Muscle architecture of the common chimpanzee (*Pan troglodytes*): perspectives for investigating chimpanzee behavior. *Primates* **47**, 218–229.

Channon AJ, Günther MM, Crompton RH, et al. (2009) Mechanical constraints on the functional morphology of the gibbon hind limb. *J Anat* **215**, 383–400.

Channon AJ, Crompton RH, Günther MM, et al. (2010) Muscle moment arms of the gibbon hind limb: implications for hylobatid locomotion. *J Anat* **216**, 446–462.

D'Aout K, Aerts P, De Clercq D, et al. (2002) Segment and joint angles of hind limb during bipedal and quadrupedal walking of the bonobo (*Pan paniscus*). *Am J Phys Anthropol* **119**, 37–51.

Deloison Y (1985) Comparative study of calcanei of primates and *Pan–Australopithecus–Homo* relationship. In: *Hominid Evolution: Past, Present and Future*. (ed. Tobias P), pp. 143–147. New York: Alan R. Liss.

Delp SL, Loan JP (1995) A graphics-based software system to develop and analyze models of musculoskeletal structures. *Comput Biol Med* **25**, 21–34.

Delp SL, Hess WE, Hungerford DS, et al. (1999) Variation of rotation moment arms with hip flexion. *J Biomech* **32**, 493–501.

DeSilva JM (2009) Functional morphology of the ankle and the likelihood of climbing in early hominins. *Proc Natl Acad Sci USA* **106**, 6567–6572.

Drapeau MSM (2004) Functional anatomy of the olecranon process in hominoids and Plio-Pleistocene hominins. *Am J Phys Anthropol* **124**, 297–314.

Elftman H, Manter J (1935a) Chimpanzee and human feet in bipedal walking. *Am J Phys Anthropol* **20**, 69–79.

Elftman H, Manter J (1935b) The evolution of the human foot, with especial reference to the joints. *J Anat* **70**, 56–67.

Eng CM, Smallwood LH, Rainiero MP, et al. (2008) Scaling of muscle architecture and fiber types in the rat hindlimb. *J Exp Biol* **211**, 2336–2345.

Fleagle JG (1976) Locomotor behavior and skeletal anatomy of sympatric Malaysian leaf-monkeys (*Presbytis obscura* and *Presbytis melalophos*). *Yearb Phys Anthropol* **20**, 440–453.

Gebo DL, Schwartz GT (2006) Foot bones from Omo: implications for hominid evolution. *Am J Phys Anthropol* **129**, 499–511.

Gomberg DN (1985) Functional differences of three ligaments of the transverse tarsal joint in hominoids. *J Hum Evol* **14**, 553–562.

Graham KM, Scott SH (2003) Morphometry of *Macaca mulatta* forelimb. III. Moment arm of shoulder and elbow muscles. *J Morphol* **255**, 301–314.

Grimston SK, Nigg BM, Hanley DA, et al. (1993) Differences in ankle joint complex range of motion as a function of age. *Foot Ankle* **14**, 215–222.

Hamill J, Selbie WS (2004) Three-dimensional kinematics. In: *Research Methods in Biomechanics*. (eds Robertson DGE, Caldwell GE, Hamill J, Kamen G, Whittlesey SN), pp. 35–52. Champaign, IL: Human Kinetics.

Hintermann B, Nigg BM, Sommer C (1994) Foot movement and tendon excursion: an *in vitro* study. *Foot Ankle Int* **15**, 386–395.

Hughes RE, Niebur G, Liu J, et al. (1998) Comparison of two methods for computing abduction moment arms of the rotator cuff. *J Biomech* **31**, 157–160.

Jenkins FA (1972) Chimpanzee bipedalism: cineradiographic analysis and implications for the evolution of gait. *Science* **178**, 877–879.

Jungers WL, Susman RL (1984) Body size and skeletal allometry in African apes. In: *The Pygmy Chimpanzee: Evolutionary Biology and Behavior*. (ed. Susman RL), pp. 131–177. New York: Plenum Press.

Jungers WL, Harcourt-Smith WEH, Wunderlich RE, et al. (2009) The foot of *Homo floresiensis*. *Nature* **459**, 81–84.

Ker RF, Bennett MB, Bibby SR, et al. (1987) The spring in the arch of the human foot. *Nature* **325**, 147–149.

Kidd RS, O'Higgins P, Oxnard CE (1996) The OH8 foot: a reappraisal of the functional morphology of the hindfoot utilizing a multivariate analysis. *J Hum Evol* **31**, 269–291.

Klein P, Mattys S, Rooze M (1996) Moment arm length variations of selected muscles acting on talocrural and subtalar joints during movement: an *in vitro* study. *J Biomech* **29**, 21–30.

Latimer B, Lovejoy CO (1989) The calcaneus of *Australopithecus afarensis* and its implications for the evolution of bipedality. *Am J Phys Anthropol* **78**, 369–386.

Latimer B, Ohman JC, Lovejoy CO (1987) Talocrural joint in African hominoids: implications for *Australopithecus afarensis*. *Am J Phys Anthropol* **74**, 155–175.

Leardini A, Benedetti MG, Berti L, et al. (2007) Rear-foot, mid-foot and fore-foot motion during the stance phase of gait. *Gait Posture* **25**, 453–462.

Lewis OJ (1980a) The joints of the evolving foot. Part I. The ankle joint. *J Anat* **130**, 527–543.

Lewis OJ (1980b) The joints of the evolving foot. Part II. The intrinsic joints. *J Anat* **130**, 833–857.

Lewis OJ (1980c) The joints of the evolving foot. Part III. The fossil evidence. *J Anat* **131**, 275–298.

Lieber RL (2010) *Skeletal Muscle Structure, Function, and Plasticity: The Physiological Basis of Rehabilitation*, 3rd edn. New York: Lippincott Williams & Wilkins.

Lieber RL, Ljung B, Fridén J (1997) Intraoperative sarcomere length measurements reveal differential design of human wrist extensor muscles. *J Exp Biol* **200**, 19–25.

Lovejoy CO, Latimer B, Suwa G, et al. (2009) Combining prehension and propulsion: the foot of *Ardipithecus ramidus*. *Science* **326**, 72e1–72e8.

McCullough MB, Ringleb SI, Arai K, et al. (2011) Moment arms of the ankle throughout the range of motion in three planes. *Foot Ankle Int* **32**, 300–306.

Mendez J, Keys A (1960) Density and composition of mammalian muscle. *Metabolism* **9**, 184–188.

Myatt JP, Crompton RH, Thorpe SKS (2011) Hindlimb muscle architecture in non-human great apes and a comparison of methods for analysing inter-species variation. *J Anat* **219**, 150–166.

Nagano A (2001) A Computer Simulation Study on the Potential Locomotor Patterns of *Australopithecus afarensis* (AL 288–1). PhD Dissertation, Arizona State University.

Oishi M, Ogihara N, Endo H, et al. (2012) Muscle dimensions of the foot in the organutan and the chimpanzee. *J Anat* **221**, 311–317.

Pandy MG (1999) Moment arm of a muscle force. *Exerc Sport Sci Rev* **27**, 79–118.

Payne RC, Crompton RH, Isler K, et al. (2006a) Morphological analysis of the hindlimb in apes and humans. I. Muscle architecture. *J Anat* **208**, 709–724.

Payne RC, Crompton RH, Isler K, et al. (2006b) Morphological analysis of the hindlimb in apes and humans. II. Moment arms. *J Anat* **208**, 725–742.

Perry JMG, Wall CE (2008) Scaling of the chewing muscles in prosimians. In: *Primate Craniofacial Function and Biology*. (eds Vineyard CJ, Ravosa MJ, Wall CE), pp. 217–240. New York: Springer.

Perry JMG, Hartsone-Rose A, Wall CE (2011) The adductors of strepsirrhines in relation to body size, diet and ingested food size. *Anat Rec* **294**, 712–728.

Piazza SJ, Cavanagh PR (2000) Measurement of screw-home motion of the knee is sensitive to errors in axis alignment. *J Biomech* **33**, 1029–1034.

Polk JD (2002) Adaptive and phylogenetic influences on musculoskeletal design in cecopithecine primates. *J Exp Biol* **205**, 3399–3412.

Pontzer H, Raichlen DA, Sockol MD (2009) The metabolic cost of walking in humans, chimpanzees, and early hominins. *J Hum Evol* **56**, 43–54.

Prejzner-Morawska A, Urbanowicz M (1981) Morphology of some of the lower limb muscles in primates. In: *Primate Evolutionary Biology: Selected Papers (Part A) of the VIIIth Congress of the International Primatological Society, Florence, 7–12 July 1980*. (eds Chiarelli AB, Corruccini RS), pp. 60–67. New York: Springer.

Raichlen DA, Armstrong H, Lieberman DE (2011) Calcaneus length determines running economy: implications for endurance running performance in modern humans and Neandertals. *J Hum Evol* **60**, 299–308.

Rugg SG, Gregor RJ, Mandelbaum BR, et al. (1990) *In vivo* moment arm calculations at the ankle using magnetic resonance imaging (MRI). *J Biomech* **23**, 495–501.

Sarmiento EE, Marcus LF (2000) The os navicular of humans, great apes, OH 8, Hadar, and *Oreopithecus*: function, phylogeny, and multivariate analyses. *Am Mus Novit* **3288**, 1–38.

Schultz AH (1963) Relations between the lengths of the main parts of the foot skeleton in primates. *Folia Primatol* **1**, 150–171.

Siegler S, Chen J, Schneck CD (1988) The three-dimensional kinematics and flexibility characteristics of the human ankle and subtalar joints – part I: kinematics. *J Biomech Eng* **110**, 364–373.

Sinclair J, Taylor PJ, Edmundson CJ, et al. (2012) Influence of the helical and six available Cardan sequences on 3D ankle joint kinematic parameters. *Sports Biomech* **3**, 430–437.

Smith RJ, Jungers WL (1997) Body mass in comparative primatology. *J Hum Evol* **32**, 523–559.

Sockol MD, Raichlen DA, Pontzer H (2007) Chimpanzee locomotor energetics and the origin of human bipedalism. *Proc Natl Acad Sci USA* **104**, 12 265–12 269.

Sokal RR, Rohlf FJ (2012) *Biometry*, 4th edn. New York: W.H. Freeman.

Spoor CW, van Leeuwen JL (1992) Knee muscle moment arms from MRI and from tendon travel. *J Biomech* **25**, 201–206.

Spoor CW, van Leeuwen JL, Meskers CGM, et al. (1990) Estimation of instantaneous moment arms of lower-leg muscles. *J Biomech* **23**, 1247–1259.

Stern JT, Susman RL (1983) The locomotor anatomy of *Australopithecus afarensis*. *Am J Phys Anthropol* **60**, 279–317.

Strasser E (1992) Hindlimb proportions, allometry, and biomechanics in Old World monkeys (Primates, Cercopithecidae). *Am J Phys Anthropol* **87**, 187–213.

Susman RL (1983) Evolution of the human foot: evidence from Plio-Pleistocene hominids. *Foot Ankle* **3**, 365–376.

Susman RL, Stern JT, Jungers WL (1984) Arboreality and bipedality in the hadar hominids. *Folia Primatol* **43**, 113–156.

Swindler DR, Wood CD (1973) *An Atlas of Primate Gross Anatomy, Baboon, Chimpanzee and Man*. Seattle, WA: University of Washington Press.

Thorpe SK, Crompton RH, Gunther MM, et al. (1999) Dimensions and moment arms of the hind- and forelimb muscles of common chimpanzees (*Pan troglodytes*). *Am J Phys Anthropol* **110**, 179–199.

Thorpe SKS, Crompton RH, Wang WJ (2004) Stresses exerted in the hindlimb muscles of common chimpanzees (*Pan troglodytes*) during bipedal locomotion. *Folia Primatol* **75**, 253–265.

Trinkaus E (1983) *The Shanidar Neandertals*. New York: Academic Press.

Venkataraman VV, Kraft TS, Dominy NJ (2013) Tree climbing and human evolution. *Proc Natl Acad Sci USA* **110**, 1237–1242.

Ward SR, Eng CM, Smallwood LH, et al. (2009) Are current measurements of lower extremity muscle architecture accurate? *Clin Orthop Relat Res* **467**, 1074–1082.

Winter DA (2005) *Biomechanics and Motor Control of Human Movement*. Hoboken, NJ: Wiley.

Yamazaki N, Ishida H, Kimura T, et al. (1979) Biomechanical analysis of primate bipedal walking by computer-simulation. *J Hum Evol* **8**, 337–349.

Young JW (2005) Ontogeny of muscle mechanical advantage in capuchin monkeys (*Cebus albifrons* and *Cebus apella*). *J Zool* **267**, 351–362.

Zajac FE (1989) Muscle and tendon: properties, models, scaling, and application to biomechanics and motor control. *Crit Rev Biomed Eng* **17**, 359–411.

Zipfel B, DeSilva JM, Kidd RS, et al. (2011) The foot and ankle of *Australopithecus sediba*. *Science* **333**, 1417–1420.